Acta Geophysica
https://doi.org/10.1007/s11600-022-00921-5

RESEARCH ARTICLE - APPLIED GEOPHYSICS

Integration of feature extraction, attribute combination and image segmentation for object delineation on seismic images

Keyvan Khayer[1] · Esmail Hosseini Fard[1] · Amin Roshandel Kahoo[1] · Mehrdad Soleimani Monfared[1,2] · Alireza Ahmadyfard[3]

Received: 5 May 2021 / Accepted: 3 September 2022

Abstract

Automatic geological interpretation, specifically modeling salt dome and fault detection, is controversial task on seismic images from complex geological media. In advanced techniques of seismic interpretation and modeling, various strategies are utilized for combination and integration different information layers to obtain an image adequate for automatic extraction of the object from seismic data. Efficiency of the selected feature extraction, data integration and image segmentation methods are the most important parameters that affect accuracy of the final model. Moreover, quality of the seismic data also affects confidence of the selected seismic attributes for integration. The present study proposed a new strategy for efficient delineation and modeling of geological objects on the seismic image. The proposed method consists of extraction specific features by the histogram of oriented gradients (HOG) method, statistical analysis of the HOG features, integration of features through hybrid attribute analysis and image classification or segmentation. The final result is a binary model of the target under investigation. The HOG method here modified accordingly for extraction of the related features for delineation of salt dome and fault zones from seismic data. The extracted HOG parameter then is statically analyzed to define the best state of information integration. The integrated image, which is the hybrid attribute, then is used for image classification, or image segmentation by the image segmentation method. The seismic image labeling procedure performs on the related seismic attributes, evaluated by the extracted HOG feature. Number of HOG feature and the analyzing parameters are also accordingly optimized. The final image classification then is performed on an image which contains all the embedded information on all the related textural conventional and statistical attributes and features. The proposed methods here apply on four seismic data examples, synthetic model of salt dome and faults and two real data that contain salt dome and fault. Results have shown that the proposed method can more accurately model the targets under investigation, compared to advanced extracted attributes and manual interpretations.

Keywords Seismic interpretation · Attribute integration · Feature extraction · HOG · Image segmentation

Edited by Dr. Seyed Yaser Moussavi Alashloo (ASSOCIATE EDITOR) / Prof. Gabriela Fernández Viejo (CO-EDITOR-IN-CHIEF).

✉ Amin Roshandel Kahoo
roshandel@shahroodut.ac.ir

Keyvan Khayer
k.khayer@shahroodut.ac.ir

Esmail Hosseini Fard
hoseinifardesmail@gmail.com

Mehrdad Soleimani Monfared
msoleimani@shahroodut.ac.ir;
mehrdad.soleimani@partner.kit.edu

Alireza Ahmadyfard
ahmadyfard@shahroodut.ac.ir

[1] Department of Mining, Petroleum and Geophysics Engineering, Shahrood University of Technology, Shahrood, Iran

[2] Geophysical Institute (GPI), Karlsruhe Institute of Technology (KIT), Karlsruhe, Germany

[3] Department of Electrical and Robotic Engineering, Shahrood University of Technology, Shahrood, Iran

Published online: 20 September 2022

Introduction

Geological interpretation based on geophysical data is the state-of-the-art of integrating various source of information to build the most accurate and geologically plausible model of the subsurface structures. Generally, delineation the geometry and root of diapirs such as salt or mud diapirs, requires integration of various seismic attributes (Shafiq et al. 2017; Amin and Deriche 2015). The general way is to enhance resolution of the seismic image, extract seismic attribute and integrate their embedded information. As an advantage in advanced integration and interpretation method, the final image has to be appropriate for accurate automatic geological interpretation. Accurate automatic delineation model of complex geological targets, such as salt or mud diapirs, is an interested target in seismic image analysis, subsurface geological studies and natural resource explorations (Amin et al. 2017). Upward movement of competent layers such as salt or mud, and their intrusion into the adjacent layers, complicates the geometry of diapirs. This movement also dislocates large mass of fluids and sediments and makes diapir related structures such as anticline or listric normal faults (Shafiq et al. 2018). The geometry of the root and boundaries of diapirs and its interaction with adjacent sediments, which cannot accurately imaged and interpreted by conventional analyzing methods, supposed to be better identified using information integration of seismic attributes (Velidou et al. 2015; Soleimani 2016a; Amin and Deriche 2016). Glinskii et al. (2008) mapped geometry of two mud volcanoes in the Taman mud-volcanic province by seismic measurements. They improved the earth model of the mud volcanos by numerical simulation of seismic images. Somoza et al. (2012) analyzed the mud volcanoes in the western Alboran Sea and stated that accurate shape delineation and exact boundary modeling requires high resolution seismic data and intensive interpreter interaction. By investigation on mud diapir on the Black sea, Xing and Spiess (2015) was shown that there is still deficiency in definition the exact root depth of mud volcanoes using conventional image analysis in 2D seismic images. Shafiq et al. (2015) introduced 3D gradient of texture (3D-GoT) to area selection in seismic cube based on the different seismic texture of geological events. Using advanced analyzing tools, Maestrelli et al. (2017) defined mud volcanoes and revealed that seismic texture properties can be used in 3D seismic data for semi-automatic object selection. However, availability of high-resolution 3D seismic data is questionable in the areas within the first stages of surveys. Thus, 2D seismic data are commonly used for geological interpretation and structural modeling in frontier steps of investigation (Halpert et al. 2014; Soleimani 2016b). However, poor quality of seismic image, influence on result of using conventional imaging, interpretation and integration techniques. Mauri et al. (2017) stated that structural complexity of the target in the seismic image is the most influential factor in improving accuracy of the automatic interpretation. However, there are various methods for resolving those obstacles for geological target modeling and its boundary enhancement. It was shown that geological interpretation of diapirs and their geometrical properties can be defined through integration of various information layers (Soleimani and Rafie 2016; Singh et al. 2016; Shahbazi et al. 2016, 2020; Hegazy and AlRegib 2014). As an advanced method, integration of geophysical data used for detection of salt diapirs boundary (Soleimani et al. 2018a, b) and accurate delineation of mud diapir (Soleimani et al. 2018b). Nevertheless, reduced temporal resolution, poor quality of seismic data and geometrical complexity of the target, diminish efficiency of those integration method (Di et al. 2018). An advanced proposed method for accurate image segmentation is using the histogram of orients gradients (HOG). The HOG method generally applies for image analysis such as face recognition (Shu et al. 2011), moving activity recognition on videos (Aggarwal and Xia 2014), landmine detection in ground-penetrating radar (Torrione et al. 2014), event recognition on magnetic resonance imaging (MRI) data (Ahmed et al. 2017) and also for automatic tuberculosis screening in chest radiographs (Vajda et al. 2018). The HOG method also apples to define simple 2D planar objects, such as fault, in integration with other methods, such as supervised machine learning algorithm (Guitton et al. 2017). One of the most important geological structures that is of great importance in exploration studies are faults. Fault structures can create structural traps by shifting the stratification. Therefore, the study of fault structures is important. Sometimes due to structural complexity and noise in seismic data, identifying the fault plane is a difficult process and it is not possible to determine their exact location. As mentioned above, seismic attributes are tools that reveal information contained in seismic data and allow the seismologist to interpret quantitatively. Bahorich and Farmer (1995) using coherence attribute detected faults in three-dimensional seismic data. Roberts (2001) detect the fault in 3D seismic data by curvature attribute. Tingdahl and De Rooji (2005) detected the fault boundary by combining three attributes similarity, frequency and curvature by artificial neural network method. Boe and Daber (2010) extracted the curvature attribute from seismic data and then combined result volume with RGB color blending for detecting the structural information in seismic data. Aqrawi and Boe (2011) used the modify Sobel attribute for detecting fault in 3D seismic data. Zheng et al. (2014) combined the similarity, curvature and spectral decomposition attributes

with artificial neural network. Guo et al. (2018) detected the fault in seismic data by using the convolutional neural network and compere the result with independent methods. Hosseini-Fard et al. (2022) introduced a strategy for automatic geological interpretation on seismic images. Mousavi et al. (2022) presented a novel strategy for fault enhancement in seismic images and they compare the result with other approach.

To resolve the problem of complex geological object delineation on seismic image, the presented study proposes to modify the HOG method for application on seismic data. Thus, the HOG method here is modified to extract structural characterization and textural properties of geological object from seismic image. The main concern of this study is that the HOG by itself is not sufficient to discriminate between structures in a seismic image. Therefore, here is proposed to use statistical analysis of the HOG parameters for further accurate analysis. Also, through the attribute and feature extraction, a separate attribute as the hybrid texture attribute is also introduced. In the following the HOG method is analyzed for application of complex geological object delineation on seismic images. Then the proposed methodology is presented and applies on four seismic data (two synthetic data and two real data) examples containing complex geological objects. The first data example contains a salt dome, the second contains the fault and the third data contain the salt dome and fault. The HOG parameters are extracted for each data example, the statistical analysis is performed, followed by the integration procedure. Afterwards, an image classification tools is applied on the integrated image to define the geometry of the salt dome and fault on each seismic image. Results for each data are also compared and evaluated by results of other advanced interpretation methods and also manual interpretation on seismic images.

The proposed methodology by HOG

The proposed method in this study consists of extracting the HOG features, deriving statistical parameters related to texture attributes and delineation of the target by integration of selected images. The key of image segmentation in seismic images is the approach used to define the features, which is the main contribution of the proposed method. Magnitude distribution and angle of gradient are the basis of the HOG features, for classification of any desired object in image. Initially a filter applied on the seismic image (SI), to estimate the gradient in image. This filter is normally selected as:

$$h_x = [-1, 0, 1], \tag{1a}$$

$$h_y = [-1, 0, 1]^T. \tag{1b}$$

The results of applying these filters on seismic image are two gradient images as:

$$g_x = \mathrm{SI} * h_x, \tag{2a}$$

$$g_y = \mathrm{SI} * h_y, \tag{2b}$$

where * shows the convolution operator. For each pixel of these two gradient images, extracted originally from seismic image, two important parameters for each pixel are extracted. These parameters are the magnitude of the gradient and the angle of the dominant gradient as:

$$G(i,j) = \sqrt{g_x^2(i,j) + g_y^2(i,j)}, \tag{3a}$$

$$\theta(i,j) = \tan^{-1}\left(\frac{g_y(i,j)}{g_x(i,j)}\right), \tag{3b}$$

where $G(i,j)$ is the gradient magnitude and $\theta(i,j)$ represents the angle of the dominant gradient. The latter parameter differs from one seismic image to another, based on the continuity of reflectors of the geological objects and orientation of its features. These raw parameters obtained from the images are further processed to be used for image segmentation. Orientation binning applies also as the next step. Orientation binning consists of binning the image, normalizing and projecting the magnitude of gradients. The orientation binning process performs between $g_y = \frac{-\pi}{2}$ and $\frac{+\pi}{2}$. In large seismic data, and specifically in the presence of random noise in data, which disturb clear identification of gradient orientation, individual pixels are merged to produce a group of pixels known as the cell. Similarly, combination of histogram of oriented gradients of merged pixels defines the same parameter in the cell. Before combination of pixel parameter into a cell, the magnitudes need to be normalized. According to the seismic image size, the computation time considerations, the level of image contamination by noise and the desired accuracy of modeling details of the structure, a group of cells can be merged to build a block (Naseer 2020). The same procedure for parameter combinations and normalizations considerations, need to be accounted for. Subsequently, the gradient orientation and the magnitude of gradient in each cell or block of the seismic image are obtained. These parameters are then used for feature extraction. Figure 1a shows an example of deriving the HOG parameter of a seismic image. To extract the HOG parameter on predefined blocks of seismic image, a survey sketch of the sliding window needs to be defined. The general way is to design a 9×9 or 16×16 sliding window, which slides over the image from one corner point to the other, with or

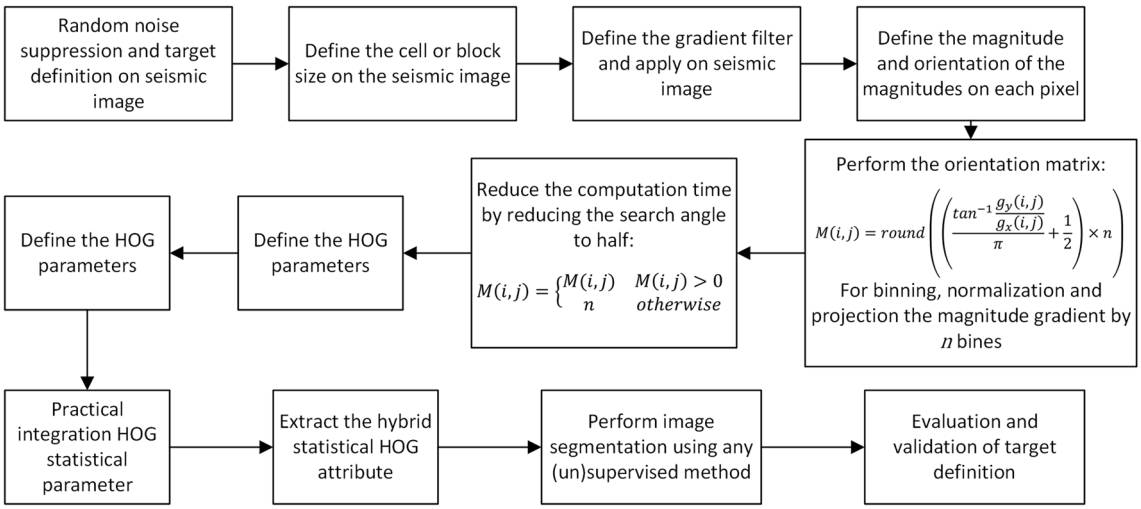

Fig. 1 The simplified stepwise flowchart of the proposed method

without multi coverage of pixels or cells. Figure 1b shows four different seismic patter that might be all observed in a single window. According to the textural properties of the geological object in seismic image, individual representation or integrated illustrations of these HOG statistical parameters better enhances the target. The proposing statistical parameters here are the mean, minimum, maximum, variance, product, kurtosis and skewness of HOG values. It practically sounds to extract faults in seismic data using the statistical minimum and/or maximum HOG values. Also, the chaotic patterns in seismic images might be related to the salt or fault in seismic images. The statistical variance HOG parameter can also be used for better identification of the object boundary. However, it should be noted that any combination of statistical parameters needed to be practically analyzed (Di and AlRegib 2020). As a result of practical analysis in this study, here is proposed to use a combination of maximum, minimum, mean, and variance HOG statistical parameters in each image block for boundary identification of geological objects, such as salt dome or faults. The combination of these HOG statistical parameter here is known as the hybrid attribute $H_{B(i,j)}$:

$$H_{B(i,j)} = \frac{\mu_{B(i,j)}}{\left[\delta_{B(i,j)} \times \left(\alpha_{B(i,j)} - \beta_{B(i,j)}\right)\right] + \varepsilon}. \quad (4)$$

This attribute is define for determining the salt dome boundary, where $\alpha_{B(i,j)}$ shows the maximum, $\beta_{B(i,j)}$ represents the minimum, $\mu_{B(i,j)}$ represents the mean, and $\delta_{B(i,j)}$ shows the variance value. The parameter ε is also added to prevent possible division by zero. The $H_{B(i,j)}$ attribute section is an appropriate input section for the next step of using a supervised or unsupervised image classification, to provide a binary image of the target under investigation. There is no preference here in selection of supervised or unsupervised methods for applying on the extracted hybrid attribute image. Here is proposed to use the support vector machine (SVM) method to classify the pixels. Nevertheless, it is also possible to perform unsupervised learning strategies to solve the same problem, or some strategies between supervised or unsupervised learning methods (Chen 2017; Kumar and Mandal 2018). Similar to the steps mentioned above, all steps are taken to determine the fault, with the difference that the value of $H_{B(i,j)}$ is determined.

The simplified stepwise algorithm proposed in this study for 2D HOG statistical parameter analysis on seismic image comes in Fig. 1.

Delineation of salt dome by HOG

The first field data example is a seismic image containing a salt dome, surrounded by horizontal and dipping reflectors. The data used in this section are divided into two categories: synthetic data and real data. Synthetic data is the SEAM Phase I Earth Model, which is a generalized 3D representation of petroleum interests in the deep-water Gulf of Mexico. The synthetic model used in this study is part of SEAM Interpretation Challenge synthetic data. The complete seismic cross section of this model is drawn in Fig. 2a. The black rectangle drawn on this section is part of the model used in this study. The purpose of selecting this rectangle is to reduce the volume of calculations and their processing time.

According to the aim of the study, relevance attributes for evaluation of the HOG extraction procedure are selected for application on synthetic and real data. The

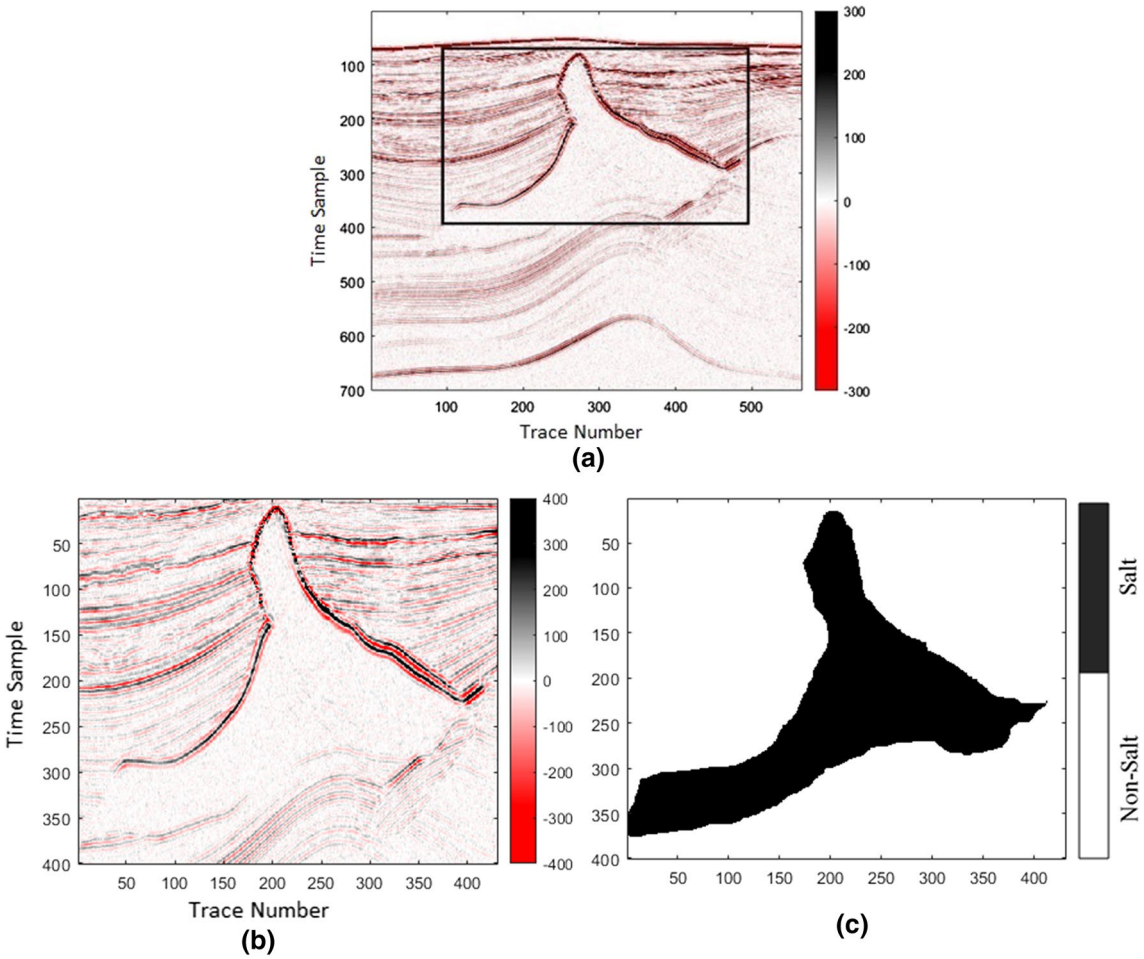

Fig. 2 **a** An inline from the 3D SEAM Interpretation Challenge synthetic data, **b** the selected subsection of the seismic image, and **c** the binary model. Data is licensed under ©2013 by SEG Advanced Modeling Corporation, SEAM Open Data

proposed method for HOG feature extraction and further image segmentation for salt dome definition are subsequently applied on the selected data example. It is supposed that the proposed method produces realistic image of the body of the salt dome, since there is no specific internal reflector within the salt. The proposed method separates areas with different seismic texture in seismic image. Generally, top of the salt dome is easily detected by the HOG features. It is due to the sharp boundary between the salt dome and upper layers, as areas with two different HOG features. To extract the HOG features from the seismic images, it is required to label the seismic image in advance. These labels are used for further classification and statistical analysis of the HOG parameters within each seismic pattern. To better select different seismic pattern on seismic image and accurate labeling, the instantaneous phase attribute used here (Fig. 3b). Four different seismic patterns are labeled on the seismic image, illustrated in Fig. 3a. In the next step, two other important HOG application parameters, which are the window size and number of features are analyzed. To define the optimum window size, large number of values with various number of features were analyzed. The appropriate value for the selected window size and number feature are equal to 5 and 6, respectively.

As can be seen in Fig. 3, the maximum and minimum attributes performed poorly in identifying the bottom of the salt dome (Fig. 3b and c). Also, the range and mean attributes did not have a high ability to identify the bottom of the salt dome. The variance attribute (Fig. 3e) and the product attribute (Fig. 3f) performed better in identifying the salt dome boundary than the other attributes, but they were also unable to identify the salt dome floor. The kurtosis (Fig. 3g) and skewness (Fig. 3h) parameters detect the side boundaries of the salt dome.

More investigation results reveal that using the new proposed hybrid texture attribute probably increases accuracy of salt dome boundary detection. Result of applying the new hybrid texture attribute is shown in Fig. 4a. The salt dome here is depicted with more accuracy than any other attribute.

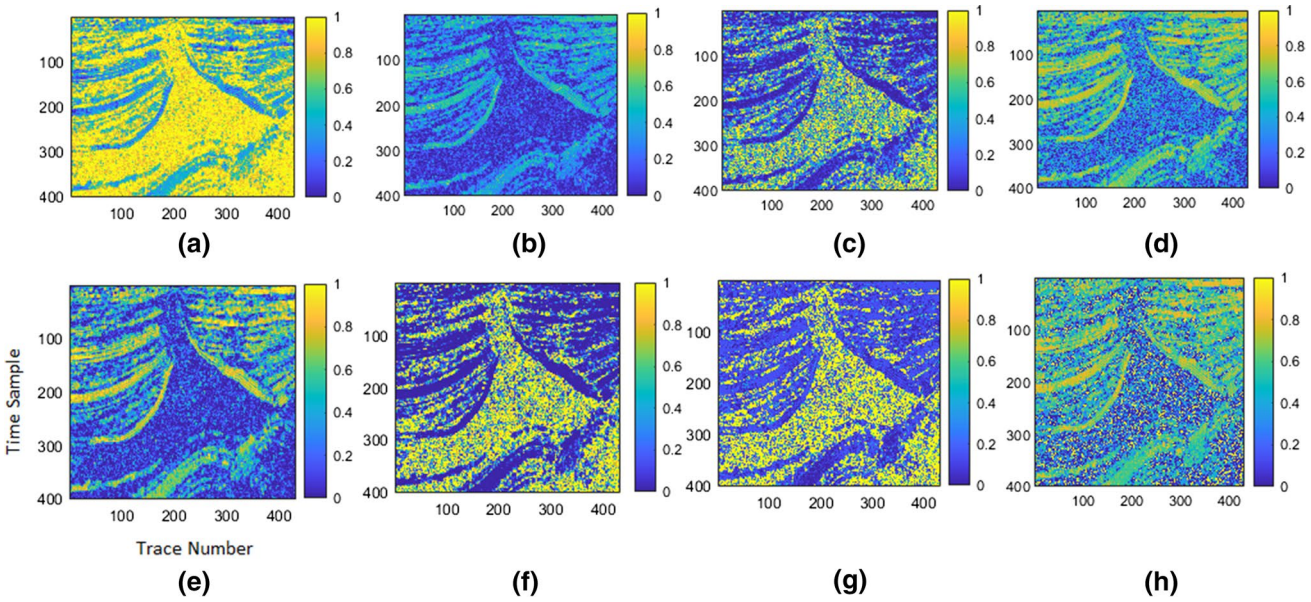

Fig. 3 The result of HOG attribute: **a** mean, **b** maximum, **c** minimum, **d** range, **e** variance, **f** product, **g** kurtosis, and **h** skewness. All vertical axes represent time in seconds and horizontal axes represent distance in meter

For quantitative evaluation of the images, they need to be converted to binary models. This conversion was performed by applying automatic thresholding and morphological correction methods in MATLAB software. Figure 4b shows the binary model obtained from the hybrid attribute. Also, to compare the accuracy of the proposed method with other conventional classification methods, the salt dome boundary was determined using SVM method. Figure 4c shows the binary model obtained from SVM method.

For accuracy evaluation, result is compared by the model obtained through the manual interpretation. To calculate the accuracy, two methods of comparing pixel to pixel and F1 score were used. In the first method, by comparing the synthetic binary model pixel to pixel with the binary model obtained from the hybrid attribute, the accuracy of this attribute was determined and its value is equal to 97% and the accuracy of the SVM method is 96.4%. Sensitivity and specificity are two important indicators in statistical evaluation of the performance of binary classification test results. F1 score uses these two indicators to determine the accuracy of a method. The value of a calculated for HOG hybrid attribute is equal to 86.5% and the value for SVM method is 85.8%. Nevertheless, accuracy of salt boundary detection by automatic interpretation here is comparable with manual interpretation. However, bottom salt boundary in manual interpretation is under question, which resolved here by proposed method. Figure 5b shows the edge content attribute and Fig. 5c shows the chaos attribute for evaluation of the proposed method (Fig. 5a), which shows consistency between results.

The performance of the proposed attribute on a real seismic salt dome data was also examined. Figure 6a shows the seismic sections of the real salt dome along with its binary model, which in this study, part of this data has been used, which is shown with a black box on it. Figure 6b is the intended data from the section of Fig. 6a. Figure 6c is the binary model that result of the average interpretations made by three experienced interpreters. The seismic data is selected from NLOG, Dutch oil and gas portal. The selected line relates to the M block in the North Sea, the Dutch section, and the selected line is 84A209. First, HOG attributes were extracted from the data shown in Fig. 7. The appropriate value for the selected window size and number feature are equal to 27 and 45, respectively. The HOG attributes mean, minimum and maximum that shown in Fig. 7a–c detect the texture of salt dome and have not been very successful in identifying the boundary of the salt dome. The HOG attributes variance, product, range, skewness and kurtosis each shows a part of the salt dome boundary in Fig. 7d–h, respectively.

As can be seen in the attribute shown in Fig. 7, none of the attributes alone are able to identify the salt dome, especially its boundary. Therefore, HOG hybrid attribute was generated using Eq. 4. Figure 8 shows this attribute along with the binary model. Similar to the synthetic model, the value of accuracy was calculated using two methods of comparing pixels to pixels and F1 score method. The value of accuracy from comparing the pixels is 94.36% and the value of F1 score is 82.68% which are acceptable values.

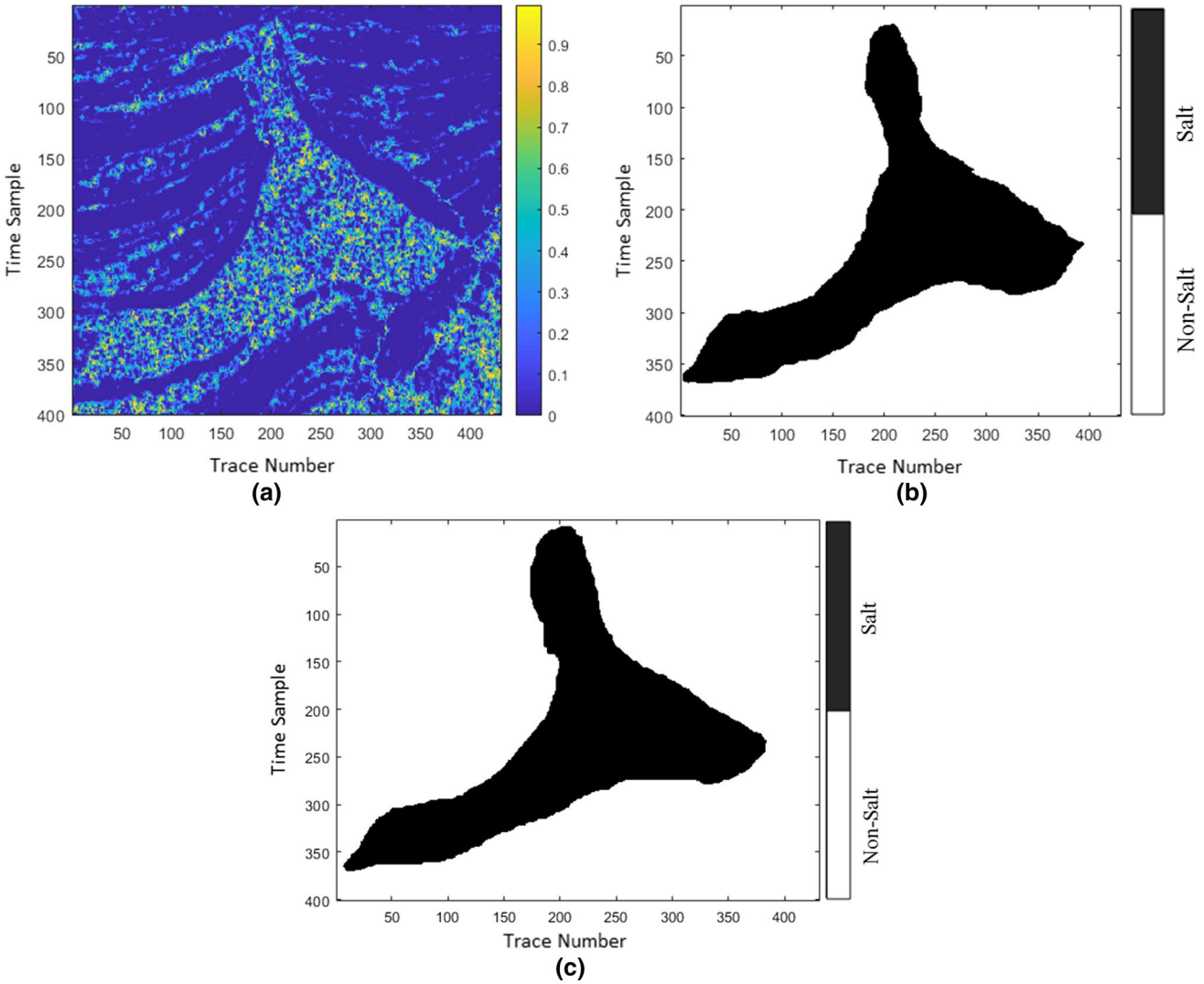

Fig. 4 **a** The Hybrid attribute, **b** the binary model from hybrid attribute that obtained by segmentation, and **c** the binary model obtained by the SVM method

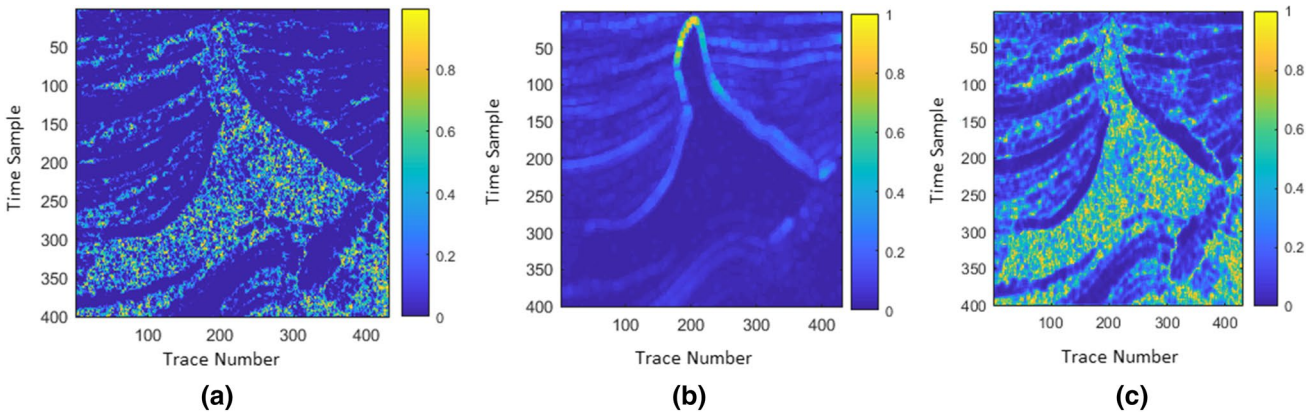

Fig. 5 **a** HOG hybrid attribute, **b** edge content attribute, and **c** chaos attribute

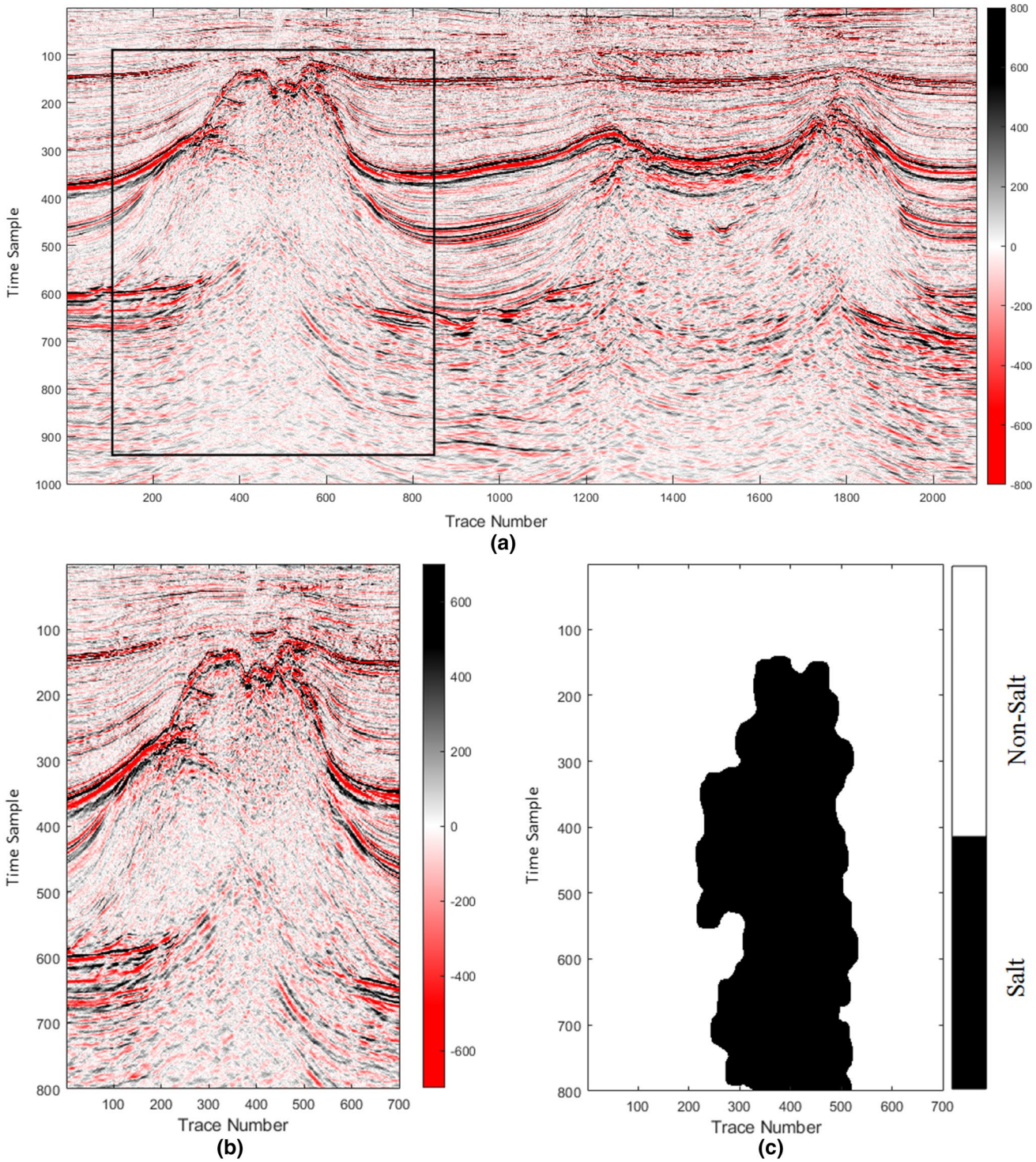

Fig. 6 **a** Seismic section of real salt dome, **b** selected real seismic data in this study, and **c** the binary model of real salt dome obtained from manual interpretation. Data are from NLOG, Dutch oil, and gas portal, selected from M block, line 84A209

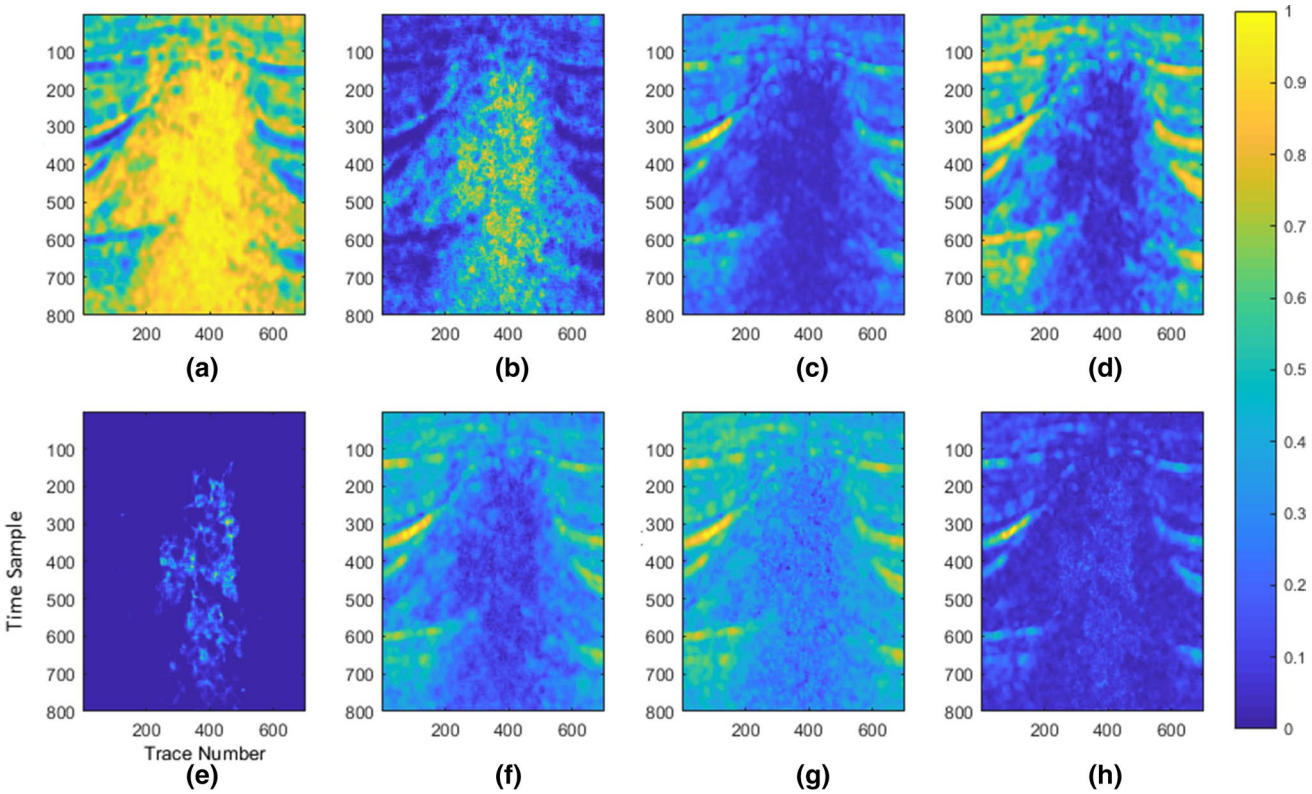

Fig. 7 The HOG attributes: **a** mean, **b** minimum, **c** maximum, **d** variance, **e** product, **f** range, **g** skewness, and **h** kurtosis

Figure 9 compares the hybrid attribute produced with other attributes such as chaos attribute and edge content attribute in same size window. As can be seen, the HOG hybrid attribute has defined the boundary and texture of the salt dome better than the other two attributes and is less affected by the surrounding layers, which indicates the high ability of this attribute to determine the boundary of the salt dome.

Delineation of fault by HOG

As mentioned in the previous sections, identifying the location of major and minor faults in seismic sections is another challenge for interpreter. One of the tools that help to identify the location of faults in seismic sections is seismic attributes. Many seismic attributes help achieve this goal, but none alone can detect the exact location of faults. According to the results obtained from HOG attributes and HOG hybrid in identifying the salt dome boundary's, it was decided to evaluate the efficiency of this attribute in identifying the location of the fault in this study. For this purpose, first a synthetic model with main and secondary faults was prepared, which can be seen in the figure of 10 seismic sections. The selected seismic data here is a part of the data (Fig. 10b) that known as the BP 2007 synthetic data (Fig. 10a), which is created by Hemang Shah and is provided courtesy of BP Exploration Operation Company Limited ("BP").

In order to extract the HOG attributes from the synthetic model, many size of the window and number feats were examined and finally a window with size 9 and number feature 25 was selected as the optimal parameters of the attribute. Therefore, using these two parameters, HOG attributes were extracted from the synthetic model which are shown in Fig. 11. As shown in Fig. 11, kurtosis, maximum, range, and variance attributes (Fig. 11a, b, f, and h) have almost the same behavior, mean and skewness attributes (Fig. 11c and g) have acted almost similarly, and minimum and product attributes (Fig. 11d and e), unlike the salt dome, are not very effective in detecting faults.

Depending on how each of the HOG attributes works in identifying the fault, similar to the salt dome, a relation can be obtained to produce the hybrid attribute. For this purpose, according to Fig. 12, four windows of the same size in two fault and non-fault zones were considered and the values of each of the HOG attributes are prepared according to Table 1.

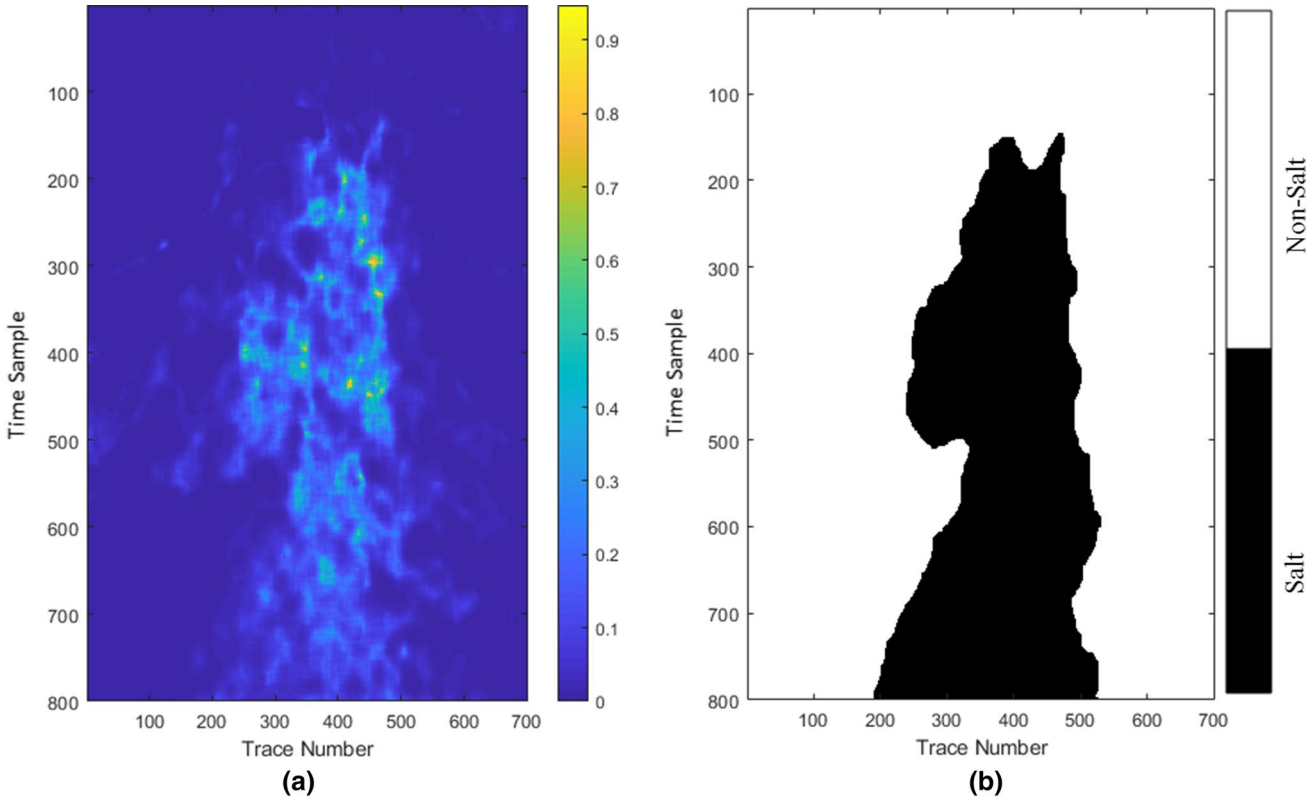

Fig. 8 **a** The HOG hybrid attribute, and **b** binary model of HOG hybrid attribute

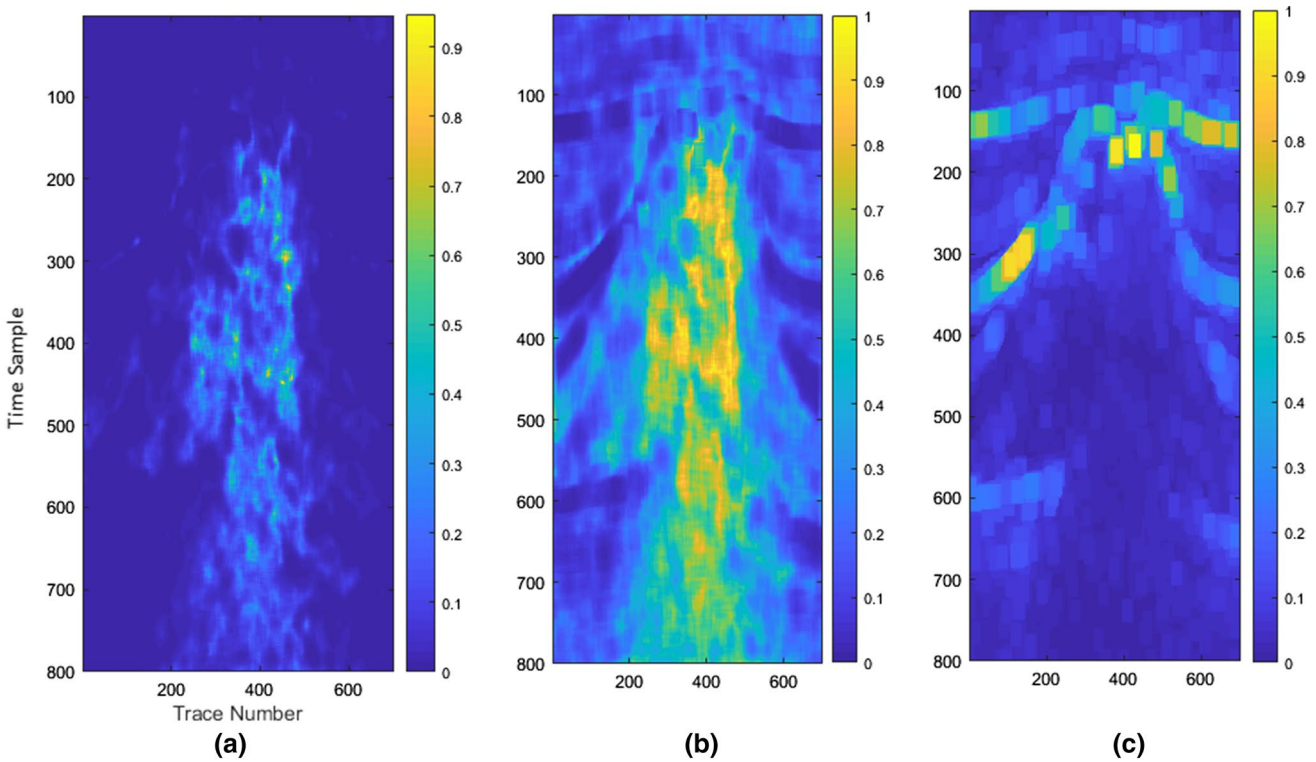

Fig. 9 **a** HOG hybrid attribute, **b** chaos attribute, and **c** edge content attribute

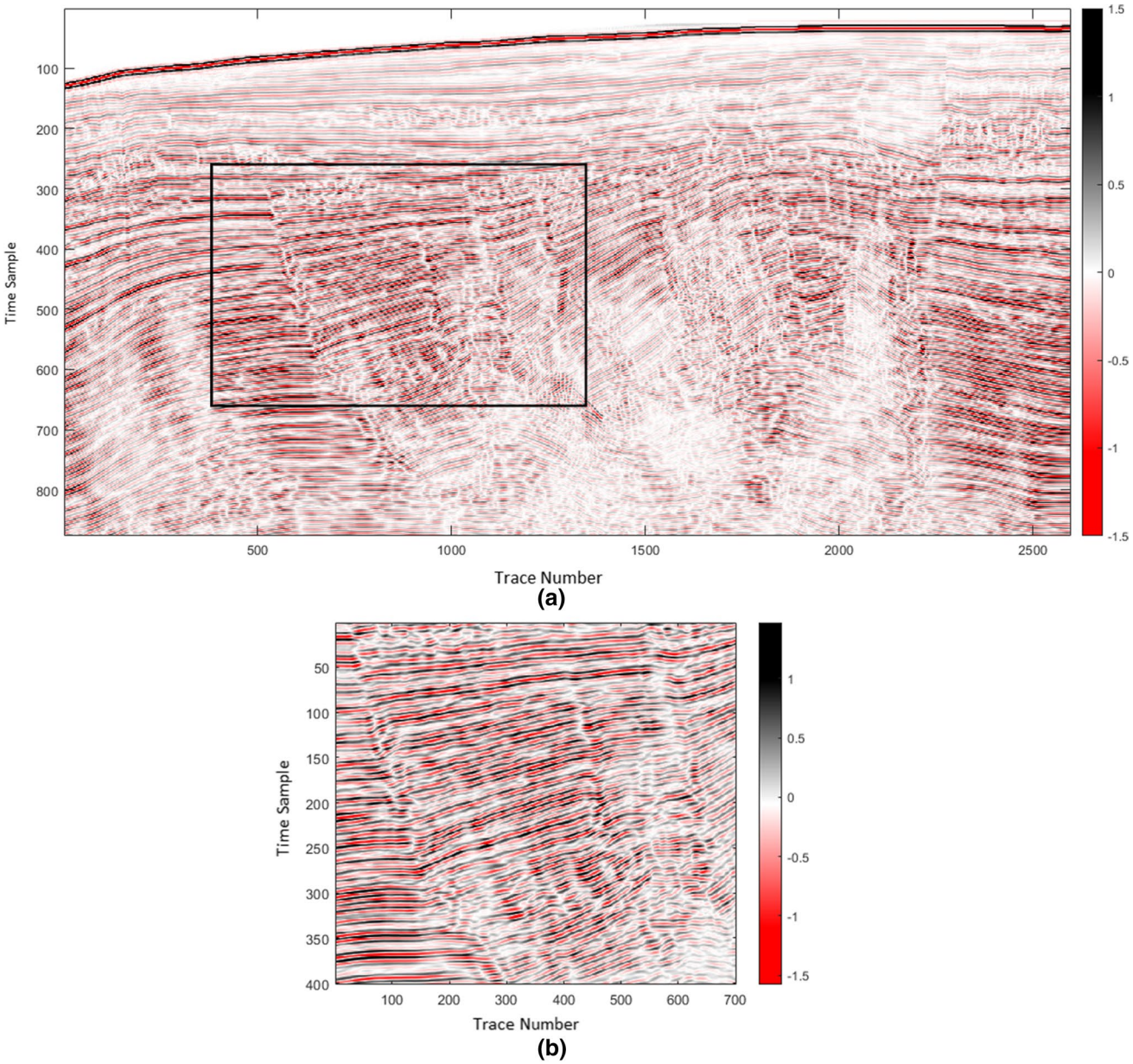

Fig. 10 **a** The seismic section, and **b** the selected subsection for the study. This data was created by Hemang Shah and is provided courtesy of BP Exploration Operation Company Limited ("BP")

As can be seen in Table 1, the values of the three parameters kurtosis, mean and variance have the most differences compared to other parameters in fault and non-fault zones, so using these three parameters, the fault zone can be determined relative to non-fault. By examining the mathematical relationships that can be established between these parameters, the best mathematical relationship in order to identify the fault zone is:

$$H_{B(i,j)} = \frac{\text{Variance}(i,j)}{((\text{kurtosis}(i,j) - \text{mean}(i,j))^2}. \quad (5)$$

Figure 13 shows the results obtained from this HOG hybrid attribute. As can be seen in the figure, this attribute has performed better in determining the fault zone than the other attributes shown in Fig. 11, and the position of the main and secondary faults has been better identified.

This method was also investigated on other a real seismic data that has faults. Figure 14 shows the seismic sections related to this data. The selected data is known as the Kerry 3D seismic data, which is available from New Zealand GNS website. All the steps implemented on the synthetic data have been performed on this data as well.

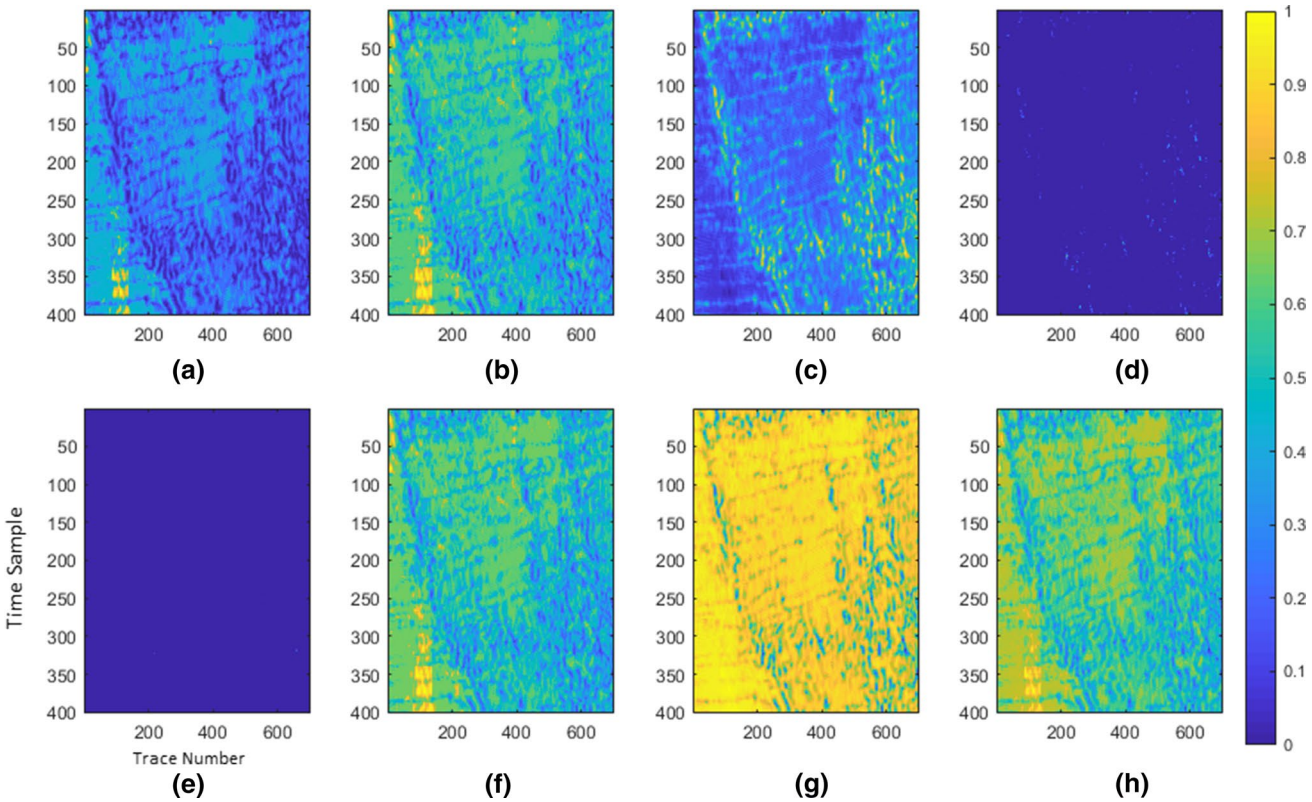

Fig. 11 HOG attributes extracted from fault synthetic model: **a** kurtosis, **b** maximum, **c** mean, **d** minimum, **e** product, **f** rang, **g** skewness, and **h** variance

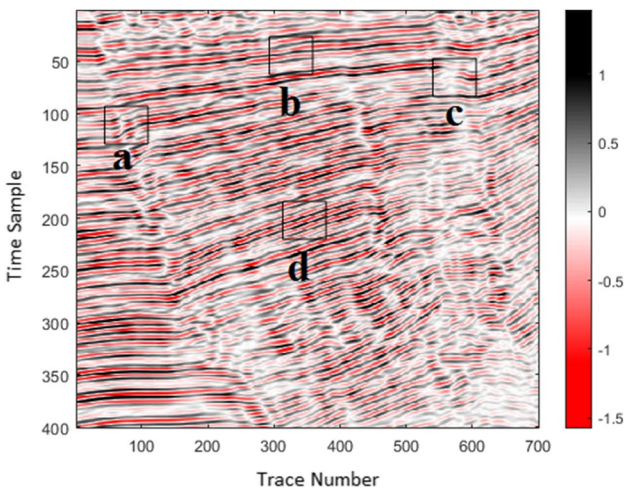

Fig. 12 Windows intended for checking their data in HOG attributes

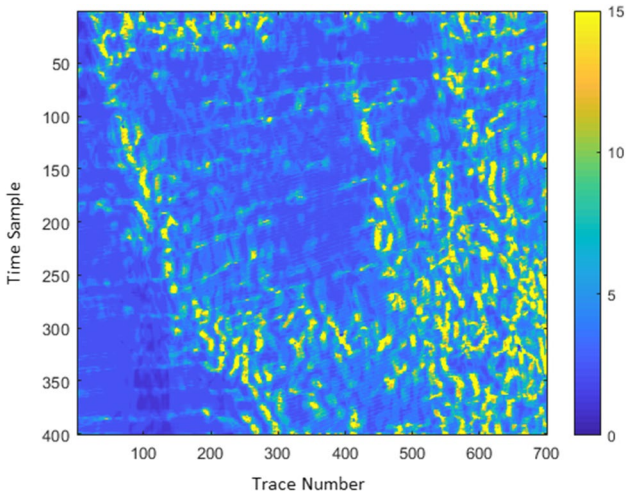

Fig. 13 HOG hybrid attribute for detecting the fault zone

For this data, the most suitable window sizes and number feature are 5 and 15, respectively. Finally, HOG attributes are extracted from real data, the results can be seen in Fig. 15. As can be seen, in general, this attribute has a good ability to determine the position of fault zones, because despite the large number of faults in a relatively small range, each fault is well separated from each other. The behavior of the four attributes mean, range, skewness and variance are similar to each other (Fig. 15c, f, g, h) and the behavior of the attribute's kurtosis, minimum, maximum and product are similar to each other (Fig. 15a, b, d, e).

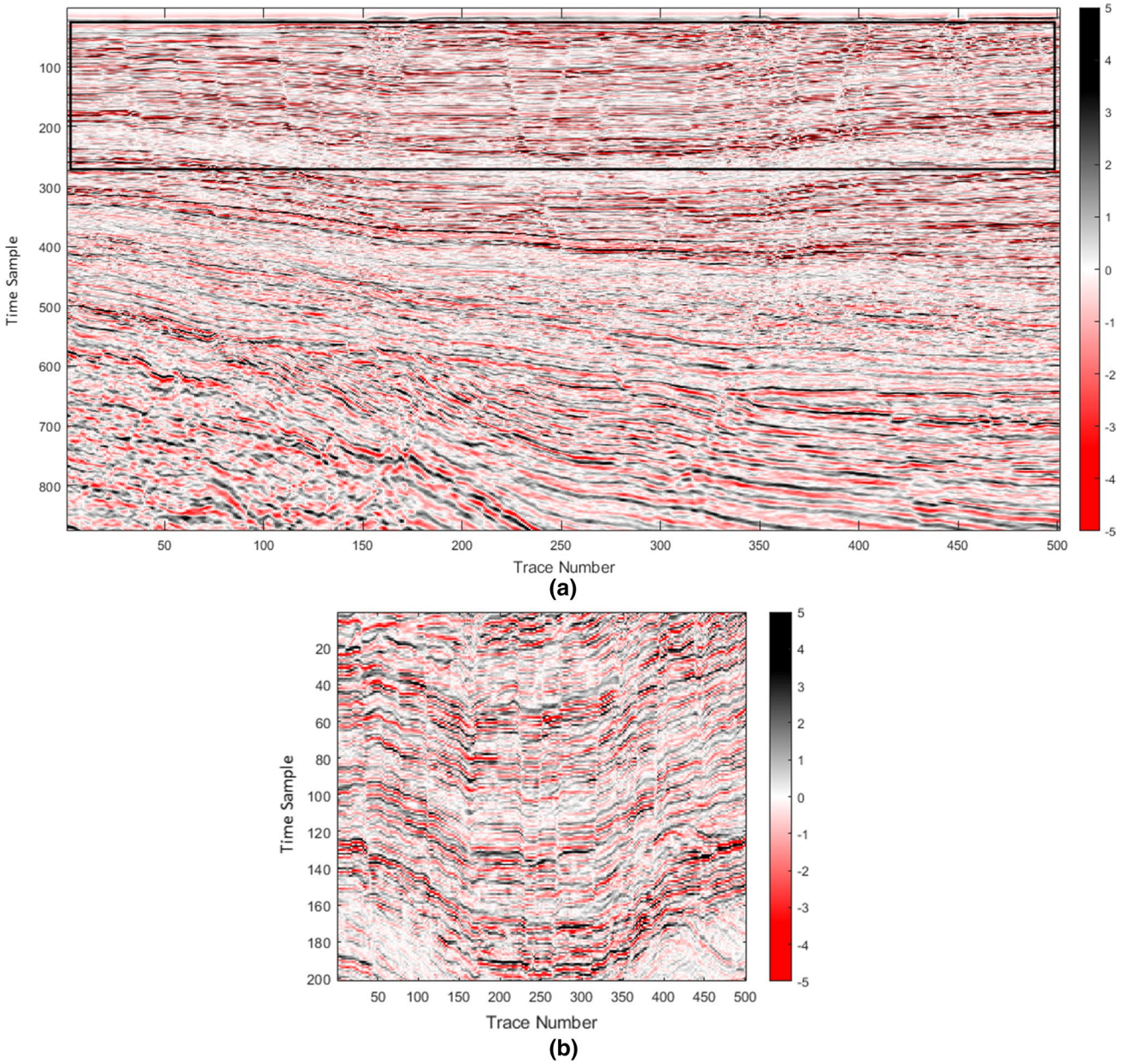

Fig. 14 **a** The seismic section of the real field data, and **b** the selected sub section. Data is Kerry 3D, available from the New Zealand Petroleum and Minerals (NZPM), the New Zealand GNS website

Using Eq. 5, HOG hybrid attribute is extracted from the real data and shown in Fig. 16a. The advantage of this attribute compared to other attributes that shown in Fig. 15 is that this attribute is not affected by background layers, which has caused the position of faults to be better displayed. In order to qualitatively compare the results obtained from

Table 1 Statistical parameters of HOG attribute in 4 windows

Seismic	Kurtosis	Mean	Max	Range	Skewness	Variance	Zone
Figure 12a	0.0384	0.5661	0.1881	0.2616	0.344	0.5856	Fault zone
Figure 12b	0.3339	0.1699	0.5513	0.592	0.6574	0.9171	Non-fault zone
Figure 12c	0.033	0.634	0.1747	0.2491	0.3172	0.5089	Fault zone
Figure 12d	0.407	0.1578	0.6039	0.6398	0.7058	0.9247	Non-fault zone

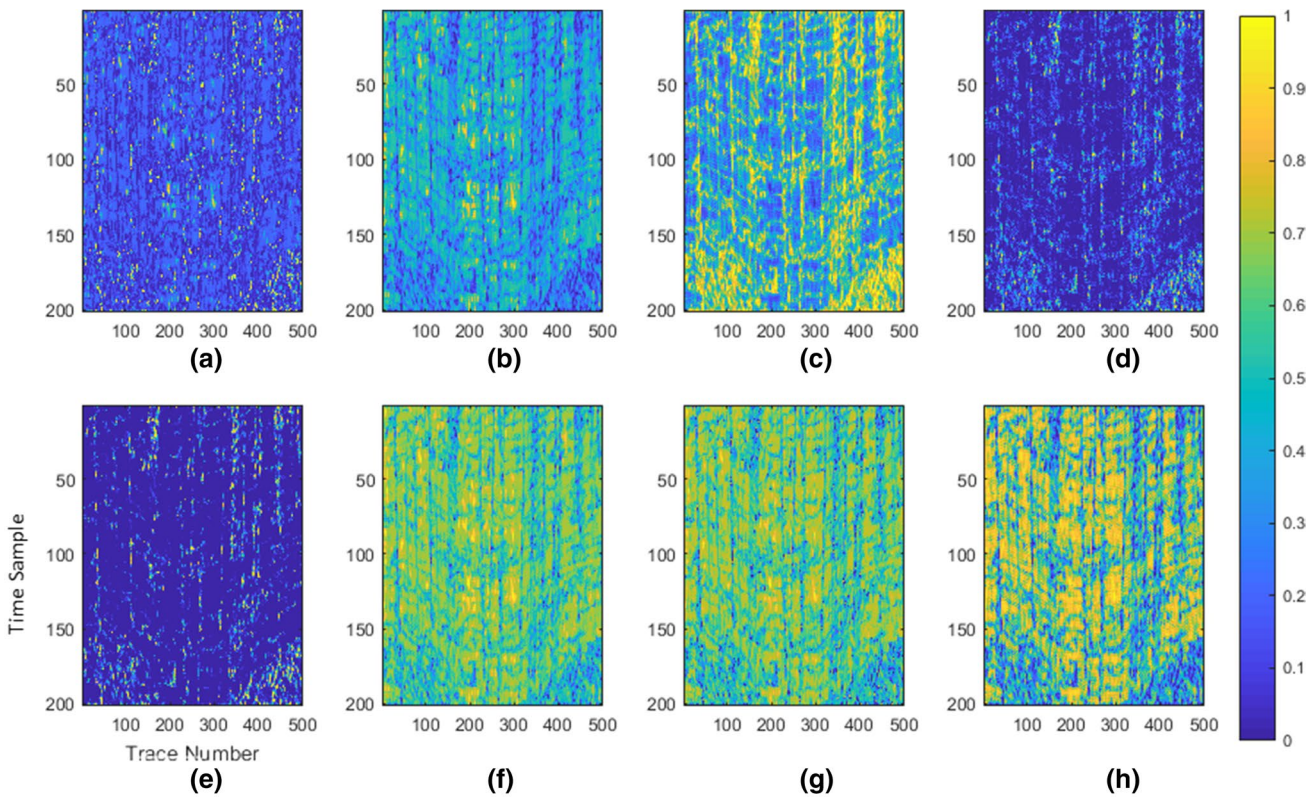

Fig. 15 The HOG attributes that extracted from real fault seismic data: **a** Kurtosis, **b** maximum, **c** mean, **d** minimum, **e** product, **f** range, **g** skewness, and **h** variance

this attribute with common attributes, the Sobel attribute extracted from this data is shown in Fig. 16b. As it is clear from the qualitative comparison of the two, the hybrid attribute has determined the location of the faults more accurately than the Sable attribute.

Discussion on results and methodology

There are available wide diverse attributes for the selected purpose, whether texture or non-texture based. To derive the proposed approached, a wide literature study was performed for selecting the most appropriate attributes for salt dome automatic selection from seismic data (Berthelot et al. 2011, 2013; Amin et al. 2015; Lobos et al. 2016). Hence, the most well-known applicable attributes were analyzed in the background and only the attribute with the best performance presented here for comparison. The background analysis was not restricted only to the non-texture-based attributes; however, these attributes can somehow predict the salt dome and fault in the first and third data examples, respectively. It should be noted that in the first data example, high quality of synthetic salt dome seismic data and sufficient contrast between the salt dome and the surrounding media, allows better prediction of salt dome using various attributes. However, the third data example is the synthetic fault seismic data where many major and minor faults have appeared. Considering selection of the optimized parameters for applying the methodology on seismic data, there is no specific algorithm available for defining optimum window size and number of features. But there are some general considerations for selection of the window size on HOG. Generally, the size of the window depends on the size of the object under investigation in the seismic image (Chen et al. 2016). Small objects, such as thin salt dome with narrow width (diameter in 3D) or fault, require small window size. Obviously, large geological objects require larger window size for application of extraction of the HOG features. Small window size provides sharper boundary and larger window size, smoothen the object's boundaries in the final image. Small window size is also much more sensitive to the random noise in data, while larger window size is robust against random noise. The computation time is another issue that should be considered. Obviously large window size increases the computation time in each step. However, reducing the percentage of coverage in adjacent sliding windows, reduces the total computation time. Analysis have shown that small sliding window size with the same coverage percent between neighboring

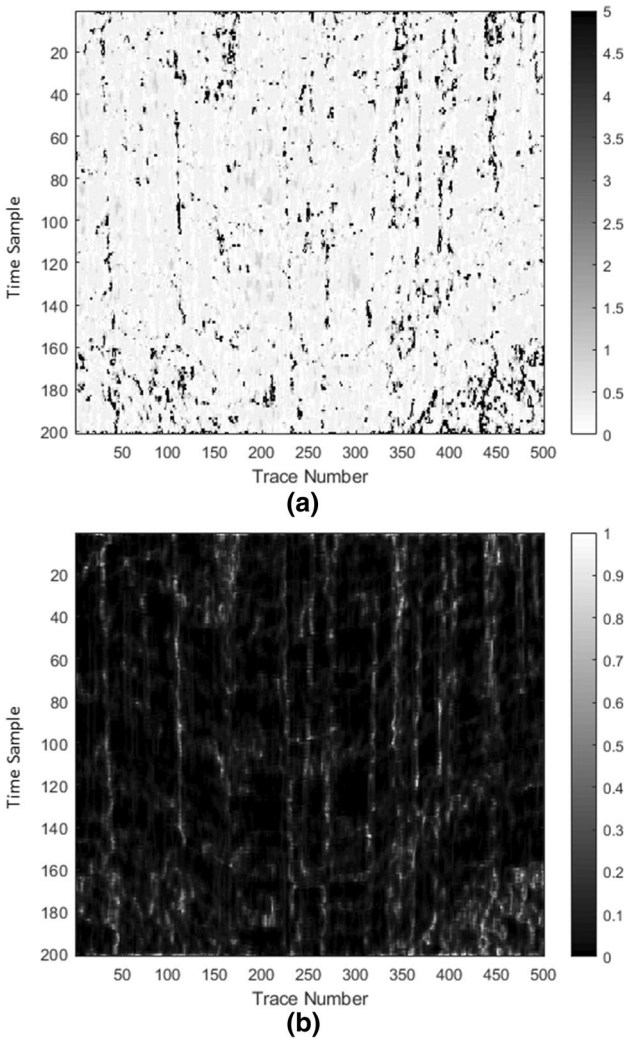

Fig. 16 **a** HOG Hybrid attribute extracted from fault real seismic data, and **b** Sobel attribute

windows, increases the total computation time. But it is not a deterministic task and should be defined during application in each individual seismic data. In the specific parallel algorithm and availability of HPC in this study, preference is to use small window size for fault detection and large window size for salt dome detection. In the first data example, since the salt dome in seismic image is rather large, thus larger window size selected for better identification of salt boundary. In the third data, since fault have narrow widths, thus small window size used to attain higher resolution in the final image. Nevertheless, seismic data in the third data example suffers from higher level of random noise, which required using small window size by care. The other important parameter in the presented method, is the number of features. There is no specific algorithm available for selection optimum number of features. Nevertheless, as a general consideration, small number of features smooths the final image, reduce the computation time and lessen sensitivity to irrelevant small objects. Large number of features, however, is more sensitive to random noise, increases the computation time and increases level of confidence in selection of the specific object under investigation. Therefore, in clean seismic data with HPC available and for large data set, preference is to use large number of features. However, it should be analyzed that how the result might differ when large number of features are used, in comparison with result using smaller number of features. The background analysis has shown that for clean data with simple structure, 30 features might obtain high quality result. However, same results, or very close to that, can be also achieved by even 10 features. It is possible that by tolerating minor error, same result with 5 features would be obtained, but saving large computation time and unnecessary calculations. So, it is mostly a tradeoff between the cost and the quality of result. For these specific data examples used in this study, application of small window size resulted to blurred image with interaction of irrelevant object, especially in top of the salt dome. Using small window size for the third data example, the location of fault zones is well defined. Obviously, parameter selection becomes more complicated when diverse geological objects with different geometrical properties are present in a single seismic image. In such circumstances, a unique window size and feature number does not attain to high quality result for both objects. Thus, the only alternative is to separate image and apply the proposed strategy in separate images. In the next step, several windows are selected in different attributes positions (target and non-target) and based on the statistical values of the attributes in each window, a suitable mathematical relation will be considered to produce a hybrid attribute. The other major concern about the accuracy of result and prediction confidence in salt dome area selection by the automatic methods arise from the labeling step. There is diversity of methods available for labeling, such as the convolutional neural network (CNN)-based methods combined by the *k*-means clustering (Kumar and Sain 2018; Chen et al. 2019). However, one should practically investigate performance of each method on diverse type of seismic data to find whether they will complicate the issue or they will suppress the problem. Soleimani and Shokri (2015) and Soltani et al. (2017) stated that any unsupervised labeling on seismic image, strongly depends on the random noise content of the data, quality of the seismic image, complexity in the geometry of the target under investigation and the contrast level between the geological object and its surrounding media. Van Gent et al. (2011) and Farrokhnia et al. (2018) also stated that presence of internal reflection in geological objects (e.g.,

impurities in salt dome), intrusion of mud or salt into the enclosed media (e.g., salt glaciers and horizontal intrusion of mud in mud diapir) and interdigitated boundary of the object reduced performance of unsupervised labeling. All these parameters complicate application of unsupervised labeling on seismic data. However, for large 3D seismic data, supervised labeling might require excessive human interaction, which increase the final total cost and computation time. Obviously, for clean seismic data with simple shaped geological object under investigation, unsupervised labeling provides acceptable results. But care should be taken in seismic data with specifications mentioned above. Therefore, it is a tradeoff between using supervised and unsupervised labeling method on seismic data base on the above-mentioned criteria (Zhang et al. 2018; Qu et al. 2019). Considering the above-mentioned criteria, the SVM classification method was selected for this study, after analyzing performance of other classification methods. It should be noted that quantitative comparison of the results can be done by comparing the ratio of the numbers of pixels defined as salt dome, to the true number of pixels definitely known as the exact salt dome.

Conclusion

Application of the integration method on the HOG extracted statistical parameters showed that the proposed methods gives reliable model of the complex geological object under investigation. Comparison of results with the proposed method and the manual interpretation and also other individual and combined attributes, revealed that the proposed method can define that target boundary and fault zone with higher accuracy. This is specifically an advantage for the salt dome with unclear root and bottom boundary. The final model of the target obtained by the proposed method also stated that the proposed method, resolve the obstacle of low-quality seismic image and unclear boundary for accurate geological interpretation on seismic images.

Acknowledgements We need to thank the individuals and companies whose data we have used in this study as fallows: Salt dome synthetic data: SEG Advanced Modeling Corporation © 2013 by SEG Advanced Modeling Corporation SEAM. These data are licensed under a Creative commons attribution 4.0 International License.

Data availability Salt dome real data: Data are from NLOG, Dutch oil and gas portal, selected from M block, line 84A209. Fault synthetic data: These data were created by Hemang Shah and are provided courtesy of BP Exploration Operation Company Limited ("BP"). Fault real data: Data name is Kerry 3D that is available from the New Zealand Petroleum and Minerals (NZPM), and the New Zealand GNS website.

Declarations

Conflict of interest The authors declare that they have no known competing financial interests or personal relationships that could have appeared to influence the work reported in this paper.

References

Aggarwal JK, Xia L (2014) Human activity recognition from 3D data: a review. Pattern Recogn Lett 48:70–80. https://doi.org/10.1016/j.patrec.2014.04.011

Ahmed S, Gillian M, Fiona CD, Rebecca MR, Scott IS, James PB (2017) Histograms of oriented 3D gradients for fully automated fetal brain localization and robust motion correction in 3 T magnetic resonance images. BioMed Res Int. ID 3956363. https://doi.org/10.1155/2017/3956363

Amin A, Deriche M (2015) A new approach for salt dome detection using a 3D multidirectional edge detector. Appl Geophys 12(3):334–342. https://doi.org/10.1007/s11770-015-0512-2

Amin A, Deriched M (2016) Salt-dome detection using a codebook-based learning model. IEEE Geosci Remote Sens Lett 13(11):1636–1640. https://doi.org/10.1109/LGRS.2016.2599435

Amin A, Deriche M, Hegazy T, Wang Z, AlRegib G (2015) A novel approach for salt dome detection using a dictionary-based classifier. In: SEG technical program expanded abstracts. Soc Exploration Geophysicists, pp 1816–1820. https://doi.org/10.1190/segam2015-5925748.1

Amin A, Deriche M, Shafiq MA, Wang Z, AlRegib G (2017) Automated salt-dome detection using an attribute ranking framework with a dictionary-based classifier. Interpretation 5(3):SJ61–SJ79. https://doi.org/10.1190/INT-2016-0084.1

Aqrawi AA, Boe TH (2011) Improved fault segmentation using a dip guided and modified 3D Sobel filter. In: SEG Technical Program Expanded Abstracts 2011 (pp. 999–1003). Society of Exploration Geophysicists. https://doi.org/10.1190/1.3628241

Bahorich M, Farmer S (1995) 3-D seismic discontinuity for faults and stratigraphic features: the coherence cube. Lead Edge 14(10):1053–1058

Berthelot A, Solberg AH, Morisbak E, Gelius LJ (2011) Salt diapirs without well defined boundaries—a feasibility study of semi-automatic detection. Geophys Prospect 59:682–696. https://doi.org/10.1111/j.1365-2478.2011.00950.x

Berthelot A, Solberg AH, Gelius LJ (2013) Texture attributes for detection of salt. J Appl Geophys 88:52–69. https://doi.org/10.1016/j.jappgeo.2012.09.006

Boe TH, Daber R (2010) Seismic features and the human eye: RGB blending of azimuthal curvatures for enhancement of fault and fracture interpretation. In SEG Technical Program Expanded Abstracts 2010 (pp. 1535–1539). Society of Exploration Geophysicists. https://doi.org/10.1190/1.3513133

Chen Y (2017) Automatic microseismic event picking via unsupervised machine learning. Geophys J Int 212:88–102. https://doi.org/10.1093/gji/ggx420

Chen Y, Huang W, Zhang D, Chen W (2016) An open-source matlab code package for improved rank-reduction 3D seismic data denoising and reconstruction. Comput Geosci 95:59–66. https://doi.org/10.1016/j.cageo.2016.06.017

Chen Y, Zhang G, Bai M, Zu S, Guan Z, Zhang M (2019) Automatic waveform classification and arrival picking based on convolutional neural network. Earth and Space Science 6:1244–1261. https://doi.org/10.1029/2018EA000466

Di H, AlRegib G (2020) A comparison of seismic saltbody interpretation via neural networks at sample and pattern levels. Geophys Prospect 68(2):521–535. https://doi.org/10.1111/1365-2478.12865

Di H, Gao D, AlRegib G (2018) 3D structural-orientation vector guided auto tracking for weak seismic reflections: a new tool for shale reservoir visualization and interpretation. Interpretation 6:SN47-SN56. https://doi.org/10.1190/INT-2018-0053.1

Farrokhnia F, Kahoo AR, Soleimani M (2018) Automatic salt dome detection in seismic data by combination of attribute analysis on CRS images and IGU map delineation. J Appl Geophys 159:395–407. https://doi.org/10.1016/j.jappgeo.2018.09.018

Glinskii BM, Sobisevich AL, Fat'yanov AG, Khairetdinov MS (2008) Mathematical simulation and experimental studies of the shugo mud volcano. J Volcanol Seismolog 2:364–371. https://doi.org/10.1134/S0742046308050060

Guitton A, Wang H, Trainor-Guitton W (2017) Statistical imaging of faults in 3D seismic volumes using a machine learning approach. SEG Technical Program Expanded Abstracts. https://doi.org/10.1190/segam2017-17589633.1

Guo B, Li L, Luo Y (2018) A new method for automatic seismic fault detection using convolutional neural network. In SEG Technical Program Expanded Abstracts 2018 (pp. 1951–1955). Society of Exploration Geophysicists. https://doi.org/10.1190/segam2018-2995894.1

Halpert AD, Clapp RG, Biondi B (2014) Salt delineation via interpreter-guided 3D seismic image segmentation. Interpretation 2(2):T79–T88. https://doi.org/10.1190/INT-2013-0159.1

Hegazy T, AlRegib G (2014) Texture attributes for detecting salt bodies in seismic data. In: SEG Technical Program Expanded Abstracts. Society of Exploration Geophysicists, pp 1455–1459. https://doi.org/10.1190/segam2014-1512.1

Hosseini-Fard E, Roshandel-Kahoo A, Soleimani-Monfared M, Khayer K, Ahmadi-Fard AR (2022) Automatic seismic image segmentation by introducing a novel strategy in histogram of oriented gradients. J Petrol Sci Eng 209:109971. https://doi.org/10.1016/j.petrol.2021.109971

Kumar PC, Mandal A (2018) Enhancement of fault interpretation using multi-attribute analysis and artificial neural network (ANN) approach: a case study from Taranaki Basin, New Zealand. Explor Geophys 49:409–424. https://doi.org/10.1071/EG16072

Kumar PC, Sain K (2018) Attribute amalgamation-aiding interpretation of faults from seismic data: an example from Waitara 3D prospect in Taranaki basin off New Zealand. J Appl Geophys 159:52–68. https://doi.org/10.1016/j.jappgeo.2018.07.023

Lobos R, Silva JF, Ortiz JM, Díaz G, Egaña A (2016) Analysis and classification of natural rock textures based on new transform-based features. Math Geosci 48:835–870. https://doi.org/10.1007/s11004-016-9648-8

Maestrelli D, Iacopini D, Jihad AA, Bond CE, Bonini M (2017) Seismic and structural characterization of fluid escape pipes using 3D and partial stack seismic from the Loyal Field, A multiphase and repeated intrusive mechanism. Mar Petrol Geol 88:489–510. https://doi.org/10.1016/J.MARPETGEO.2017.08.016

Mauri G, Husein A, Mazzini A, Irawan D, Sohrabi R, Hadi S, Prasetyo H, Miller SA (2017) Insights on the structure of Lusi mud edifice from land gravity data. Mar Pet Geol 90:104–115. https://doi.org/10.1016/j.marpetgeo.2017.05.041

Mousavi J, Radad M, Soleimani Monfared M, Roshandel Kahoo A (2022) Fault enhancement in seismic images by introducing a novel strategy integrating attributes and image analysis techniques. Pure Appl Geophys, 1–16. https://doi.org/10.1007/s00024-022-03014-y

Naseer MT (2020) Seismic attributes and reservoir simulation' application to image the shallow-marine reservoirs of Middle-Eocene carbonates, SW Pakistan. J Petrol Sci Eng 195:107711. https://doi.org/10.1016/j.petrol.2020.107711

Qu S, Guan Z, Verschuur E, Chen Y (2019) Automatic high-resolution microseismic event detection via supervised machine learning. Geophys J Int 218(3):2106–2121. https://doi.org/10.1093/gji/ggz273

Radfar A, Rahimi A, Nejati A, Soleimani M, Taati F (2018) New insights into the structure of the South Caspian Basin from seismic reflection data, Gorgan Plain. Iran Int J Earth Sci 108:379–402. https://doi.org/10.1007/s00531-018-1659-x

Roberts A (2001) Curvature attributes and their application to 3 D interpreted horizons. First Break 19(2):85–100

Shafiq MA, Wang Z, Amin A, Hegazy T, Deriche M, AlRegib H (2015) Detection of salt-dome boundary surfaces in migrated seismic volumes using gradient of textures. SEG Technical Program Expanded Abstracts 1811–1815. https://doi.org/10.1190/segam2015-5927230.1

Shafiq MA, Wang Z, AlRegib G, Amin A, Deriche M (2017) A texture-based interpretation workflow with application to delineating salt domes. Interpretation 5:SJ1–SJ19. https://doi.org/10.1190/INT-2016-0043.1

Shafiq MA, Di H, AlRegib G (2018) A novel approach for automated detection of listric faults within migrated seismic volumes. J Appl Geophys 155:94–101. https://doi.org/10.1016/j.jappgeo.2018.05.013

Shahbazi A, Ghosh D, Soleimani M, Gerami A (2016) Seismic imaging of complex structures with the CO-CDS stack method. Stud Geophys Geod 60(4):662–678. https://doi.org/10.1007/s11200-015-0452-6

Shahbazi A, Soleimani M, Thiruchelvam V, Fei TK, Babasafari AA (2020) Integration of knowledge-based seismic inversion and sedimentological investigations for heterogeneous reservoir. J Asian Earth Sci 202:104541. https://doi.org/10.1016/j.jseaes.2020.104541

Shu C, Ding X, Fang C (2011) Histogram of the oriented gradient for face recognition. Tsinghua Sci Technol 16:216–224. https://doi.org/10.1016/S1007-0214(11)70032-3

Singh D, Kumar PC, Sain K (2016) Interpretation of gas chimney from seismic data using artificial neural network: a study from Maari 3D prospect in the Taranaki basin, New Zealand. J Natural Gas Science Eng 36:339–357. https://doi.org/10.1016/j.jngse.2016.10.039

Soleimani M (2016a) Seismic image enhancement of mud volcano bearing complex structure by the CDS method, a case study in SE of the Caspian Sea shoreline. Russ Geol Geophys 57:1757–1768. https://doi.org/10.1016/j.rgg.2016.01.020

Soleimani M (2016b) Seismic imaging by 3D partial CDS method in complex media. J Petrol Sci Eng 143:54–64. https://doi.org/10.1016/j.petrol.2016.02.019

Soleimani M, Rafie M (2016) Imaging of seismic data in complex structures by introducing the partial diffraction surface stack method. Stud Geophys Geod 60. https://doi.org/10.1007/s11200-015-0942-6

Soleimani M, Shokri BJ (2015) 3D static reservoir modeling by geostatistical techniques used for reservoir characterization and data integration. Environ Earth Sci 74:1403–1414. https://doi.org/10.1007/s12665-015-4130-3

Soleimani M, Aghajani H, Heydari-Nejad S (2018a) Structure of giant buried mud volcanoes in the South Caspian Basin: Enhanced seismic image and field gravity data by using normalized full gradient method. Interpretation 6:T861–T872. https://doi.org/10.1190/INT-2018-0009.1

Soleimani M, Aghajani H, Heydari-Nejad S (2018b) Salt dome boundary detection in seismic image via resolution enhancement by the improved NFG method. Acta Geod Geoph 53:463–478. https://doi.org/10.1007/s40328-018-0222-3

Soltani P, Soleimani M, Aghajani H (2017) Faults and fractures detection in 2D seismic data based on principal component analysis. Int J Mining Geo-Eng 51(2):199–207. https://doi.org/10.22059/ijmge.2017.212587.594618

Somoza L, Medialdea T, León R, Ercilla G, Vázquez JT, líFarran M, Hernández-Molina J, González J, Juan J, Fernández-Puga MC (2012) Structure of mud volcano systems and pockmarks in the region of the Ceuta Contourite Depositional System (Western Alborán Sea). Mar Geol 332:4–26. https://doi.org/10.1016/j.margeo.2012.06.002

Tingdahl KM, De Rooij M (2005) Semi-automatic detection of faults in 3D seismic data. Geophys Prospect 53(4):533–542

Torrione PA, Morton KD, Sakaguchi R, Collins LM (2014) Histograms of oriented gradients for landmine detection in ground-penetrating radar data. IEEE Trans Geosci Remote Sens 52:1539–1550. https://doi.org/10.1109/TGRS.2013.2252016

Vajda S, Karargyris A, Jaeger S, Santosh KC, Candemir S, Xue Z, Antani S, Thoma G (2018) Feature selection for automatic tuberculosis screening in frontal chest radiographs. J Med Syst 42(8):146. https://doi.org/10.1007/s10916-018-0991-9

Van Gent H, Urai JL, de Keijzer M (2011) The internal geometry of salt structures e A first look using 3D seismic data from the Zechstein of the Netherlands. J Struct Geol 33:292–311. https://doi.org/10.1016/j.jsg.2010.07.005

Velidou DS, Tolpekin VA, Stein A, Woldai T (2015) Use of gestalt theory and random sets for automatic detection of linear geological features. Math Geosci 47:249–276. https://doi.org/10.1007/s11004-015-9584-z

Xing J, Spiess V (2015) Shallow gas transport and reservoirs in the vicinity of deeply rooted mud volcanoes in the central Black Sea. Mar Geol 369:67–78. https://doi.org/10.1016/j.margeo.2015.08.005

Zhang G, Wang Z, Chen Y (2018) Deep learning for seismic lithology prediction. Geophys J Int 215:1368–1387. https://doi.org/10.1093/gji/ggy344

Zheng ZH, Kavousi P, Di HB (2014) Multi-attributes and neural network-based fault detection in 3D seismic interpretation. Adv Mater Res 838:1497–1502. https://doi.org/10.4028/www.scientific.net/AMR.838-841.1497